Applied Catalysis B: Environmental 183 (2016) 308–316

Contents lists available at ScienceDirect

Applied Catalysis B: Environmental

journal homepage: www.elsevier.com/locate/apcatb

A modular calcination method to prepare modified N-doped TiO_2 nanoparticle with high photocatalytic activity

Lei Zeng[a,b], Zhao Lu[a], Minghui Li[a], Jin Yang[a], Wulin Song[a,c,*], Dawen Zeng[a], Changsheng Xie[a]

[a] State Key Lab of Materials Forming Simulation and Die and Mould Technology, Huazhong University of Science and Technology, Wuhan 430074, PR China
[b] South University of Science and Technology of China, Shenzhen 518055, PR China
[c] Analytic and Testing Center, Huazhong University of Science and Technology, Wuhan 430074, PR China

ARTICLE INFO

Article history:
Received 15 September 2015
Received in revised form 23 October 2015
Accepted 24 October 2015
Available online 1 November 2015

Keywords:
Modular calcination
N-doped TiO_2
Benzene
Visible light
Superoxide anion radical

ABSTRACT

In this paper, a highly active modified N-doped TiO_2 nanoparticle is prepared by a novel modular calcination method. The combination among ammonia, hydrogen, air and vacuum module is investigated comprehensively. Moreover, the effect of calcination order on photocatalytic activity is also studied. The photocatalytic property of sample annealed in ammonia firstly is better than that of the sample annealed in ammonia last. NV-TiO_2 sample which is prepared by combination between ammonia and vacuum module possesses the highest photocatalytic activity towards benzene. The photodegradation result shows that 300 ppm benzene can be decomposed completely during four hour visible light illumination. The excellent photocatalytic performance is attributed to the improvement of light harvesting, charge separation and increased surface electron scavenger, simultaneously. Besides, the photocatalytic degradation reaction path of benzene demonstrates that phenol is an important intermediate product. The faster decomposition of phenol is corresponded to higher photocatalytic reaction rate. In fact, the effect of calcination order on the photocatalytic activity is embodied in differences of the amount of oxygen vacancy and surface cleanliness. These findings aid us to prepare highly efficient visible light active photocatalyst by using a simple method and deepen the understanding on the mechanism of decomposing benzene.

1. Introduction

Benzene is a widely used and essential industrial chemical. It can be found in oil paint, printing ink and leather products, which often easily dissipated into air. Its exposure may lead progressively to leukaemia and multiple myeloma. Therefore, it is urgent to find an effective solution to eliminate benzene.

Photocatalytic oxidation (PCO) of volatile organic compounds using TiO_2 based nanomaterials has attracted considerable interests due to its strong oxidation power, environmental benefit, nontoxicity, cost effectiveness and long term stability against chemical- and photo-corrision, since Fujishima–Honda effect [1] is discovered in 1972. Decades of research have indicated that PCO technology is an effective approach to remove benzene. Especially under UV light illumination, Einaga et al. [2] reported that benzene could be oxidized completely by using platinized titania photocatalyst. Liu et al. [3] found that the photocatalytic efficiency of molybedenum ion and carbon codoped TiO_2 for benzene removal was remarkably enhanced and gained the optimal Mo doping content. The enhancment of photocatalytic activity was attributed to the generation of impurity energy level, which resulted in the increased utilization of solar energy. Liu et al. [4] synthesized CdS sensitized TiO_2 film coated on fiberglass cloth and the degradation efficiency of benzene reached 92.8%. Ren et al. [5] investigated the thermo-photocatalytic degradation of benzene on Pt loaded TiO_2/ZrO_2 and considered that the thermo-photocatalytic technique had practical application foreground in the degradation of highly concentrated benzene. As we known, UV light can induce cancerization of skin, so it avoids to be used indoors. The research on photocatalytic oxidation of benzene under visible light irradiation becomes an urgent and realistic problem. Recently, visible light active photocatalyst has been widely investigated. Hu et al. [6] prepared a novel $BiVO_4/TiO_2$ heterogenous structure photocatalyst, and the conversion rate of benzene reached 92% under simulated solar light. Nassoko et al. [7] synthesized nitrogen doped TiO_2 through an EDTA modified sol–gel process and reported that the photocatalyst had high enough activity for benzene degradation. Huang et al. [8] showed that a nanocrystal heterojunction

* Corresponding author at: State Key Lab of Materials Forming Simulation and Die and Mould Technology, Huazhong University of Science and Technology, Wuhan 430074, PR China. Fax: +86 2787557453.
E-mail address: wulins@126.com (W. Song).

http://dx.doi.org/10.1016/j.apcatb.2015.10.048
0926-3373/

$LaVO_4/TiO_2$ photocatalyst exhibited strong photocatalytic activity for decomposing benzene under visible light irradiation with high photochemical stability. Apparently, there were many strategies to improve the visible light driven photocatalytic activity of TiO_2. After consulting lots of literatures, nitrogen doping was investigated intensively due to the convenience of preparation, excellent photocatalytic performance and in-depth understanding. Hence, nitrogen doping was main approach to modify photocatalytic activity of TiO_2 used in this paper.

Generally, the nitrogen doped TiO_2 (N-TiO_2) was prepared by annealing pure TiO_2 in ammonia or nitrogen in the past. In the investigation of Zhang et al. [9], Hoang et al. [10] and Chen et al. [11], the nitrogen doped TiO_2 was prepared by annealing in ammonia firstly then by H_2 reduction or O_2 oxidation. Interestingly, the photocatalytic activity of as-prepared photocatalyst enhanced obviously. Inspired by their work, a modified nitrogen doped TiO_2 prepared by modular calcination is proposed in this paper. In the modular calcination, each annealing section was regarded as a modular. Moreover, the annealing atmosphere, holding time and calcination temperature in each modular was independent of each other and can be adjusted as requirements. In our investigation, ammonia as nitrogen source was a necessary module. The optional module included oxygen, hydrogen and vacuum. The photocatalytic activity of related photocatalyst prepared by the combination of ammonia module and optional module was compared. Several interesting conclusions were drawn from the comparison, shown in Fig. S3. Firstly, the visible light driven photocatalytic activity of modified nitrogen doped TiO_2 prepared by modular calciantion method was higher than that of nitrogen doped TiO_2 annealed only in ammonia. Secondly, the photocatalytic activity of photocatalyst annealed in ammonia firstly is higher than the sample annealed in ammonia last. The last and most important was that the photocatalyst prepared by the combination of ammonia and vacuum (NV-TiO_2) exhibited the highest photocatalytic activity in all combinations. 300 ppm benzene had declined by 95.2% over NV-TiO_2 during 4 h visible light irradiation.

In this paper, the reason why calcination order affects photocatlytic activity and why NV-TiO_2 possess excellent photocatalytic property is what we want to explan clearly. After several charcterizations, the mechanism is figured out. The enhancement of photocatalytic actitivity is attributed to the paramagnetic center $\left[O - Ti^{4+} - N^{2-} - Ti^{4+} - V_O\right]$ which can promote charge carriers seperation, exists in NV-TiO_2. Moreover, it is easier for oxygen molecule to adsorb on surface of NV-TiO_2 and electrons can be scavenged to generate super oxygen anion radical. The study on degradation mechanism of benzene suggests that the photocatalytic activity is related to the presence of phenol. The faster phenol transforms, the higher the photocatalytic activity is. In summary, more oxygen vacancies exist in NV-TiO_2 result in more active oxygen species generate in NV-TiO_2. This is the basic reason why the calcination order can affect photocatalytic activity. Finally, the modular calcination method paves a new way for enhancing visible light driven photocatalytic activity of TiO_2 nanomaterial. In addition, our findings reveal that phenol is the important intermediate product in degradation process of benzene and there is a strong correlation between phenol and photocatalytic activity. It hint that the super oxygen anion radical plays an important role in photocatalytic process. These findings also deepen the understanding on the mechanism of decomposing benzene.

2. Experimental

2.1. Synthesis of photocatalyst

The pure TiO_2 was prepared by hydrothermal reaction mentioned in previous work [12]. In our group, the modular calciantion method was systematically investigated, especially for the combiantion of two modulars. In a typical procedure, the as-prepared pure TiO_2 was annealed in ammonia (99%) at 600 °C for two hours firstly (module A), then annealed in vacuum (−0.1 MPa) at the same temperature for 2 h too (module B). In addition, the flow rate of all gas (include ammonia, hydrogen and oxygen) was 200 mL/min which was controlled by rotormeter. When the heating process was over, the tube furnace cooled down to room temperature naturely, and the gained sample was denoted to NV-TiO_2. When the calcination order was inversed, the gained sample was denoted to VN-TiO_2. The pure TiO_2 was only annealed in ammonia at 600 °C for 2 h was denoted to N-TiO_2. Similarly, the pure TiO_2 annealed in ammonia firstly then in hydrogen was denoted to NH-TiO_2, HN-TiO_2 was generated by the inverse calcination order. When used ammonia and air, the as-prepared sample was called NA-TiO_2 and AN-TiO_2. The heating rate was 5 °C/min for all samples.

2.2. Material characterization

The crystal phases of samples were analyzed by X-ray diffraction with Cu Kα radiation (XRD: PANalytical B.V., Almelo, Netherlands). The morphology, structure and grain size of the samples were examined by transmission electron microscopy (TEM: FEI Tecnai G^2 F30, Netherlands). XPS with Al K X-rays radiation operated at 300 W (XPS: Kratos XSAM800 spectrometer, USA) was used to analyze the surface properties. The shift of binding energy due to relative surface charging was corrected using the C 1s level at 284.6 eV as an internal standard. The spectra were fitted using a nonlinear least-squares fitting program (XPSPEAK) with a linear background and to the 80% Gausssian/20% Lorentzian peak shape. The PL spectra were gained by using a LabRAM HR spectrometer (HORIBA Jobin Yvon, France) with a laser excitation of 325 nm. The UV–vis absorbance spectra were obtained for the dry-pressed disk samples using a Scan UV–vis spectrophotometer (PerkinElmer, Lambda 950) equipped with an integrating sphere assembly. The spectra were recorded at room temperature in air within the range 200–900 nm. The EPR spectra were registered at 120 K using a Bruker 220 SE spectrometer, at a microwave frequency of 9.8 GHz. The operando Fourier transform infrared spectrum were obtained by using a VERTEX 70 spectrography (Bruker, Germany).

2.3. Measurement of photocatalytic activity

Evolution of the photocatalysis was carried out in a self-designed closed aluminum alloy reactor. The volume of reactor is 2 L. The mass of photocatalyst was 0.10 g and well dispersed to form a thin layer over an aluminum slice (50 mm × 50 mm). The initial concentration of benzene was kept at 300 ppm for all experiments. The concentration of benzene was on-line monitored every 10 min by GC 9560 gas-phase chromatogram equipped with FID detector. The base gas was dry air supplied by air generator. A 300 W Xe lamp was put 30 cm over the reactor to irradiate the samples. For the visible light, an appropriate filter which cuts off the wavelength below 400 nm was placed on top of the reactor to remove the ultraviolet radiation from the lamp. The conversion was calculated by $(C_0 - C)/C_0$, where C is the concentration of the reactant after irradiation, C_0 is the concentration of the reactant after adsorption equilibrium but before the irradiation in the presence of photocatalyst.

2.4. In situ DRIFTS measurement

DRIFT spectra were recorded on a Bruker Tensor 27 FTIR Spectrometer equipped with a KBr beam splitter and an MCT detector working between 1000 and 4000 cm^{-1}, using an Harrick reaction chamber with KBr windows, and an Harrick DRA-2C1 diffuse

reflectance accessory spectra were recorded at a resolution of 4 m^{-1}, and 128 scans were averaged for background spectrum resulting in a time resolution of 2 min. The as-prepared sample acted as test sample, and 0.10 g specimen was mounted on the sample holder. Firstly, the specimen was scanned, then 5 μL benzene was injected into the chamber and scanned after 10 min visible light irradiation. Finally, the DRIFTS spectrum was recorded at regular time intervals (10 min) under visible light illumination. The reaction stopped after 150 min. Then, another sample followed above test steps.

3. Results and discussion

3.1. Photocatalytic activity test

The visible light driven photocatalytic degradation result of benzene is shown in Fig. 1. The NV-TiO_2 sample exhibits the most excellent photocatalytic performance. The degradation of benzene reaches 95.5% after 4 h of visible light illumination. Meanwhile, the degradation of benzene reaches to 82.1%–52.5% for VN-TiO_2 and N-TiO_2, respectively. In the other side, no photocatalyst is added and equal amounts of pure TiO_2 are employed in the contrast group. The concentration of benzene has not decreased obviously, indicating that benzene is stable under visible light illumination and the airtightness of self-designed test platform is well enough. With regard to these distinctions, the mechanism of enhanced photocatalytic activity of NV-TiO_2 and the effect of calcination order on photocatalytic activity will be explored base on the following analysis.

3.2. Morphology and microstructure

3.2.1. XRD characterization

As is well known, the crystal phase can affect the photocatalytic activity [13]. In order to confirm whether the crystal structure of as-prepared samples vary with calcination order, all samples are characterized by XRD. As shown in Fig. 2, it is obvious to see that the phase composition of N-TiO_2 and NV-TiO_2 is same to pure TiO_2, which consists of anatase (JCPDS file No. 12-2172) and brookite (JCPDS file No. 03-0380). Interestingly, the brookite disappears and rutile (JCPDS file No. 21-1276) emerges in VN-TiO_2 sample when calcination order is reversed. In addition, the shape of XRD patterns for annealed samples is more intact than pure TiO_2, and the increased peak intensity indicates that the crystallinity of annealed samples has been improved. The FWHM of main peak decreases obviously in Fig. 2, which suggests that the crystalline size increases from pure TiO_2 to VN-TiO_2. The changes of crystallinity, crystalline size and lattice constant for these four samples are estimated by profile fitting the strongest XRD peak (using XRD analysis software-X'pert high score plus), calculated by Scherer formula and Rietveld fitting, respectively. The Rietveld profile fitting of X-ray diffraction pattern of NV-TiO_2 is shown in Fig. S1. The fitting results are listed in Table. 1 and suggest that the unit cell volume of modified TiO_2 expands comparing with pure TiO_2. It hints that nitrogen atoms have incorporated into TiO_2 lattice successfully in modified TiO_2. Furthermore, comparing to N-TiO_2, the unit cell volume of NV-TiO_2 has contracted 0.24% but that of VN-TiO_2 has expanded 0.11%. It may be attributed to the formation of different defects affected by the calcination order, more characterizations will aid us brush aside the fog.

3.2.2. TEM characterization

The particle size of these samples is confirmed by transmission electron microscopy (TEM), as shown in Fig. 3. It is evident that pure TiO_2 possesses best dispersibility and smallest particle size. After calcination, the particles grow obviously. The average particle size is about 30 nm, 34 nm and 45 nm for N-TiO_2, NV-TiO_2 and VN-TiO_2, respectively. From the view of HRTEM images in Fig. 3, it is clear to see that such grains are comprised of highly crystallized anatase with lattice of 0.35 nm which is corresponding to the (1 0 1) crystallographic plane of TiO_2. It suggests that the crystal structure is not affected by calcination order and it is consistent with XRD characterization.

3.3. Chemical composition

The chemical composition and elemental valence varied with calcination order are detected by XPS analyses. The N 1s peak of all modified samples is exhibited in Fig. 4A, and different peak shapes of three samples present. The N 1s peak of N-TiO_2 can be fitted into three peaks located in 396.1 eV, 400 eV and 403.6 eV, respectively. The first peak at 396.1 eV is assigned to the substitutional nitrogen dopant due to the N 1s peak at 395.6 eV is characteristic of N^{3-} that corresponds to TiN. The N 1s peak at 395–397 eV obtained from N-doped TiO_2 has also been assigned to the Ti—N bonding by other researchers [14–17]. The second peak at 400 eV is typically assigned to the interstitial nitrogen dopant which was summarized by Fujishima et al. [18]. The peak at 403.6 eV is usually assigned to NO_x species [19]. There is only one peak located at 400.3 eV in NV-TiO_2, indicating that nitrogen atoms have incorporated into interstitial sites. For VN-TiO_2 sample, two peaks appear at 400 eV and 403.6 eV. It suggests that interstitial nitrogen dopant and surface NO_x species exist in VN-TiO_2 sample. The valence of Ti element is reflected by Ti 2p XPS spectra. From Fig. 4B, the difference between the values of Ti 2p3/2 and Ti 2p1/2 is 5.7 eV for all samples, indicating that Ti exists in form of Ti^{4+}. In addition, no peak appears at 457 eV, which demonstrate that no Ti^{3+} forms in these samples. However, the Ti 2p peak of modified TiO_2 samples shifts towards low binding energy side apparently compared with pure TiO_2. It is related to the introduction of oxygen vacancy. As we know, oxygen is much more electronegative than titanium. The electron cloud density of titanium is influenced by electronegative of adjacent atoms. The formation of oxygen vacancy induces the increase of electron cloud density, leading to the lower binding energy shift of Ti 2p peak. The shift for NV-TiO_2 sample is most obvious, hinting that the oxygen vacancy is most abundant in NV-TiO_2 sample. To analyze the data from Table 1 and XPS characterization, the lattice parameter varied with calcination order can be explained. Nitrogen atomic radius is bigger than oxygen atomic radius. Hence, the lattice expansion happens whether nitrogen atoms incorporate into substitutional site or interstitial site of TiO_2 lattice. Both substitutional nitrogen dopant and interstitial one exist in N-TiO_2 sample. However, the atomic distance is larger in *c* axis than that in *a* and *b* axis. Therefore, nitrogen atoms favor to fill the space in *c* axis to form the interstitial dopants and occupy the oxygen site in a and b axis to form the substitutional dopants. In this way, the *c* value of N-TiO_2 is much larger while *a* and *b* value is slightly larger than that of pure TiO_2. In addition, nitrogen atoms tend to occupy interstitial position due to the lower formation energy mentioned in other publications. It also explains why the intensity of N 1s peak belonged to interstitial nitrogen is stronger than that of substitutional one. After vacuum annealing, the lattice contraction occurs in NV-TiO_2 sample compared with N-TiO_2 sample. It may be ascribed to the formation of oxygen vacancies. The substitutional nitrogen dopants form in ammonia treatment then disappear in vacuum treatment, causing the decline in *a* and *b* value compared with pure TiO_2 and only interstitial nitrogen dopants exist in NV-TiO_2. For VN-TiO_2 sample, oxygen vacancies form at first, then nitrogen atoms fill the space to form interstitial nitrogen dopant. Hence, the value of lattice parameters is the biggest among mentioned samples. The NO_x species remain on surface due to annealing in ammonia at last. Therefore, intersti-

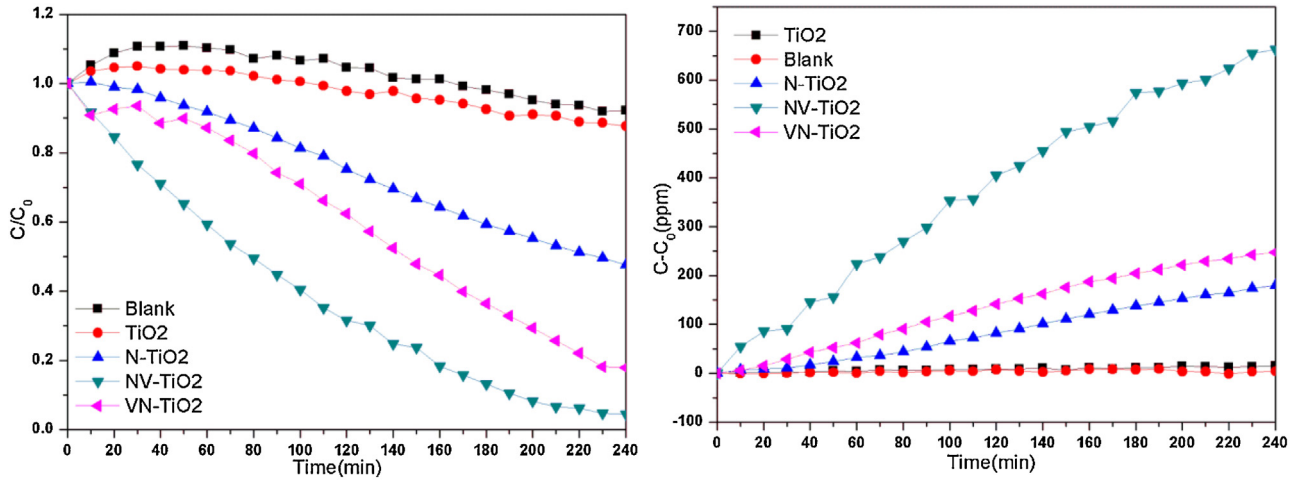

Fig. 1. Photocatalytic degradation of benzene (A) and CO_2 generation (B) by using TiO_2, N-TiO_2, NV-TiO_2 and VN-TiO_2 under visible light illumination.

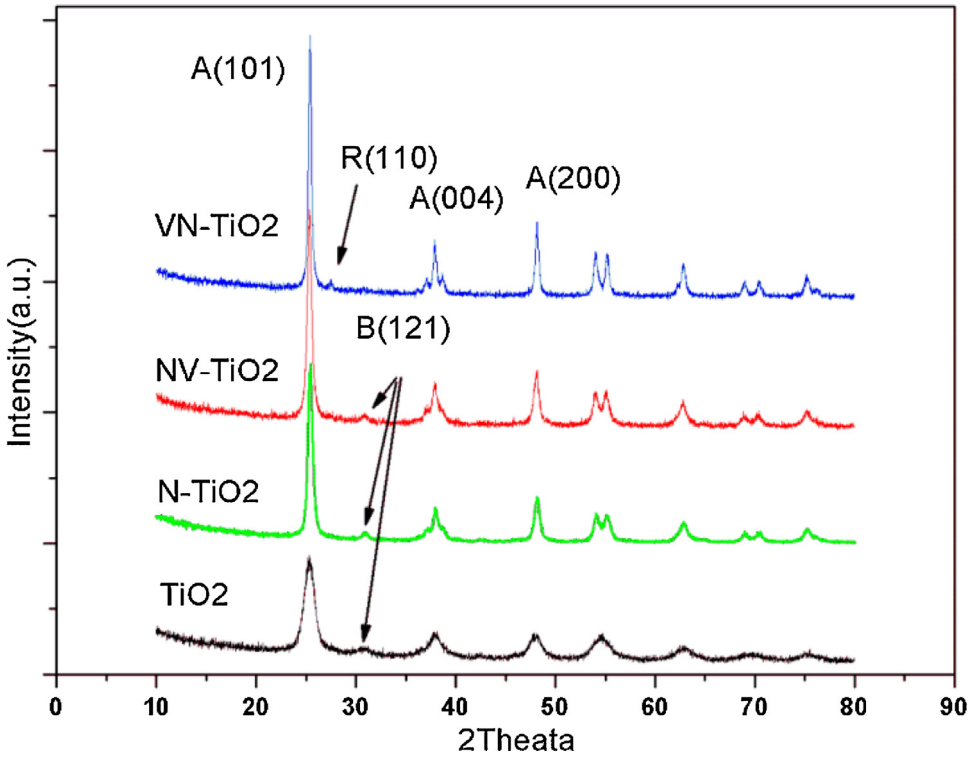

Fig. 2. XRD patterns for pure TiO_2, N-TiO_2, NV-TiO_2 and VN-TiO_2.

Table 1
The crystal parameter and XPS data for TiO2, N-TiO_2, NV-TiO_2 and VN-TiO_2.

	Crystalline size (nm)	Crystallinity (%)	Lattice parameter (Å)	Evolution factors	Nitrogen mass concentration (%)	Volume (Å3)
TiO_2	9.2	50	$a=b=3.783154$ $c=9.482553$	Rp = 15.9 Rwp = 19.1 Rexp = 14.11	-	135.716709
N-TiO_2	32.8	66.49	$a=b=3.784262$ $c=9.500809$	Rp = 22.1 Rwp = 25.7 Rexp = 21.77	0.50	136.057655
NV-TiO_2	32.6	71.7	$a=b=3.780765$ $c=9.495234$	Rp = 16.1 Rwp = 19.3 Rexp = 13.25	0.40	135.726622
VN-TiO_2	42	76.31	$a=b=3.784787$ $c=9.508714$	Rp = 15.4 Rwp = 19.0 Rexp = 15.01	0.47	136.208645

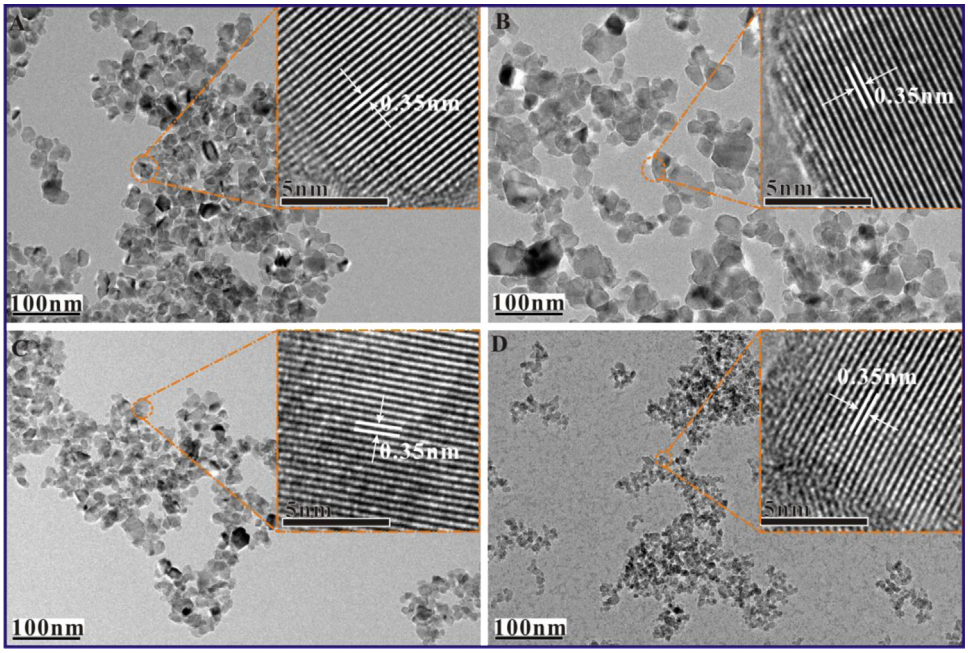

Fig. 3. TEM and HRTEM images of NV-TiO_2 (A), VN-TiO_2 (B), N-TiO_2 (C) and pure TiO2 (D).

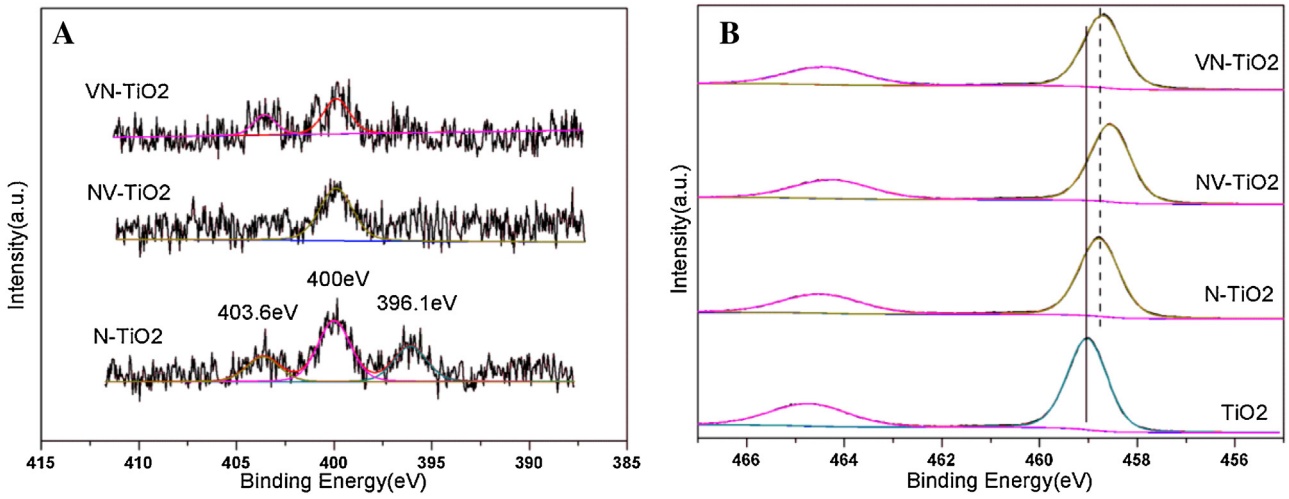

Fig. 4. *N* 1 s (A) and Ti 2p (B) XPS spectra for all modified samples.

tial nitrogen dopants and NO_x species are detected in VN-TiO_2 by XPS.

3.4. EPR characterization

The problem whether oxygen vacancy exists and what role it plays in photocatalyst still puzzles us. In order to solve the mystery, EPR technology is the preferred choice. In our experiment, three samples with equal weight are tested by EPR equipment. Fig. 5A displays EPR spectra tested in the dark. A set of signals appear at $g_1 = 2.017$, $g_2 = 1.998$, and $g_3 = 1.977$, which are characteristic signals of nitrogen doped TiO_2. The triplet g value is different from the data in previous papers. Livraghi et al. [20] have observed the triplet signal at $g_1 = 2.001$, $g_2 = 1.998$ and $g_3 = 1.927$. They assign the signals to NO_2^{2-} species originated from the reaction of NO gas with O^{2-} ions of TiO_2. However, the assignment of the nitrogen paramagnetic species to a NO_2^{2-} radical ion is inappropriate proved by theoretical calculations from Valentin et al. [21,22]. The inconsistent assignment shows an inadequate understanding of the generated EPR signal after nitridation. Because both substitutional and interstitial nitrogen dopants have theoretically similar hyperfine coupling parameters and present similar EPR signals. In this work, the intensity of EPR signals varied with calcination order and lighting condition are investigated. From Fig. 5A, it is evident to see that the triplet g value signal of NV-TiO_2 is sharpest. The peak at $g = 2.004$ which is a component of g_2 is usually assigned to oxygen vacancy with single electron. It hints that the oxygen vacancy is most abundant in NV-TiO_2. After 120 s of visible light illumination, the shape and intensity of EPR spectra changes apparently, as shown in Fig. 5B. Some weak signals located at $g_1 = 2.027$, $g_3 = 2.008$ and $g5 = 1.987$ appear in all modified samples meanwhile the triplet g value signal in N-TiO_2 becomes strongest after visible light illumination. The EPR line at $g_5 = 1.987$ is assigned to surface Ti^{3+}, indicating that photogenerated electron is trapped by surface Ti^{4+} under visible light irradiation. The EPR line at $g_1 = 2.027$ belongs to the signal of $O_2^{\bullet-}$ radical ions adsorbed on surface Ti^{4+} cations, indicating that photoexcited electrons are scavenged by oxygen in the gas phase [23]. The weak perturbation at $g_3 = 2.008$ may be

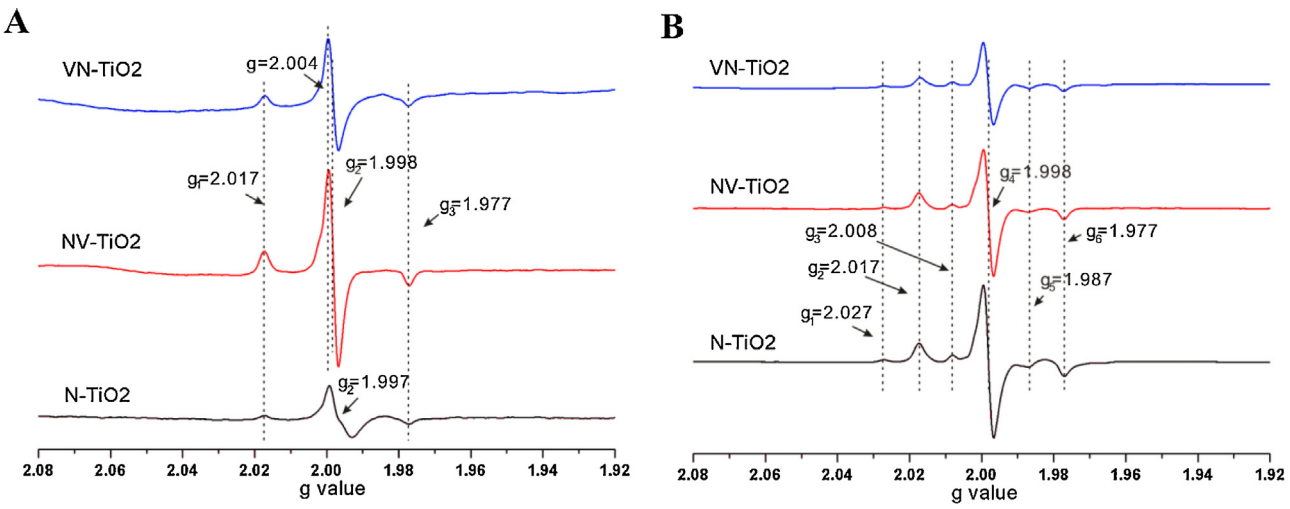

Fig. 5. EPR spectra recorded at 120 K for N-TiO_2, NV-TiO_2 and VN-TiO_2 in the dark (A) and after 120 s of visible light illumination (B).

some other unknown defect. To explain the evolution of EPR spectra, the paramagnetic center should be figured out. Zhang et al. [9] have proposed that the paramagnetic center of nitrogen doped TiO_2 is $\left[O-Ti^{4+}-N^{2-}-Ti^{4+}\right]$ and photoactive center is diamagnetic $\left[O-Ti^{4+}-N^{3-}-Ti^{3+}-V_O^-\right]$ cluster. Here, we consider that the paramagnetic center should be $\left[O-Ti^{4+}-N^{2-}-Ti^{4+}-V_O\right]$ due to the oxygen vacancy generated at high annealing temperature. More importantly, electron delocalized mobile between nitrogen anion and oxygen vacancy. Thus, the signal of oxygen vacancy traped one electron can de detected. Moreover, nitrogen atom in paramagnetic center is interstitial nitrogen dopant whereas substitutional nitrogen dopants exist as the state of diamagnetic cluster. Based on the result from XPS characterization, there are three kinds of nitrogen species in N-TiO_2 while only one nitrogen species exists in NV-TiO_2. Therefore, there are more paramagnetic centers in NV-TiO_2 than N-TiO_2. In addition, oxygen vacancies induced by vacuum treatment also contribute to the increasement of paramagnetic center. Hence, the related EPR signal in NV-TiO_2 sample is the sharpest in the dark. After visible light illumination, the related EPR signal in N-TiO_2 becomes the sharpest. It is attributed to the transformation into paramagnetic center from diamagnetic center, which exists only in N-TiO_2 comfirmed by XPS characterization. Actually, the variation of electron state leads to the evolution of EPR spectra with light illumination. For NV-TiO_2, lots of oxygen vacancies exist, which can inhibit the recombination of charge carriers and aid to transfer electron. In contrast, the electron spin state has changed due to the accumulation of paramagnetic center. Thus, the related EPR signal in NV-TiO_2 is less intense that of N-TiO_2. It suggests that the paramagnetic center in NV-TiO_2 is benefical to the separation of charge carriers.

3.5. Optical property

The optical property has closer correlation with photocatalysis. Fig. 6 shows the light harvesting ability of these samples. Compared with pure TiO_2, the red shift of absorption edge occurs obviously in modified TiO_2. NV-TiO_2 sample possess the strongest absorption in visible light region deduced by integrating the area range from 440 nm to 600 nm in UV–vis spectra. In this region, the absorption ability of VN-TiO_2 is the worst.

PL emission spectra have been widely used to investigate the efficiency of charge carrier trapping, migration, and transfer. To study the effect of calcination order on the separation efficiency of photoinduced charges, PL spectra of as-prepared samples were also investigated. As shown in Fig. 7, the PL intensity of NV-TiO_2 is the weakest among these modified samples, indicating that the separation efficiency of photoinduced charges is the best. Up to now, from the nature of material, a conclusion can be drawn. The excellent photocatalytic property of NV-TiO_2 is ascribed to good crystallinity, strong visible light harvesting ability and fast separation of electron–hole.

3.6. Study on photocatalytic degradation reaction path of benzene

Photocatalysis is a chemical reaction. Hence, not only the photocatalyst should be developed but also the reaction path need be investigated particularly. It reminders us to deeply understand the degradation mechanism of benzene. Herein, the in situ DRIFTS measurement was implemented. The DRIFTS spectrum for NV-TiO_2 sample is presented in Fig. 8. It can be found that the peak at 672 cm^{-1}, 1480 cm^{-1}, 3039 cm^{-1} and 3077 cm^{-1} which is attributed to C—H deformation vibration in benzene ring, C=C in-plane bending vibration and C—H stretching vibration [24–27], respectively, emerges after injecting benzene into reaction tank. When turning on visible light, the intensity of characteristic IR peaks of benzene weaken with the extension of reaction time, indicating that benzene is decomposed gradually. Meanwhile, a series of weak vibration strengthen gradually. It suggests that some other products generate which need to be identified further. The variation of IR peaks for N-TiO_2 and VN-TiO_2 sample displays the same trend. The only difference among these three samples is the presence of phenol, as shown in Fig. S2. The peak located at 1580 cm^{-1} is the characteristic IR peak belonging to Phenol [28]. It is observed after 10 min reaction in VN-TiO_2 while it appears after 90 min reaction in N-TiO_2. However, phenol is not detected in NV-TiO_2 during whole reaction. As we known, photogenerated hole attacks benzene and make it transform into benzene free radical [29]. Then benzene free radical reacts with hydroxyl free radical or super oxygen anion radical to produce phenol [30–32]. Phenol subsequently undergoes a series of catalytic oxidation to generate CO_2 and H_2O. In the photocatalysis process, the more the active species such as OH and O_2^- exist, the faster phenol transforms, the faster benzene is decomposed. For NV-TiO_2 sample, it is easy for oxygen molecule to adsorb on the surface, since oxygen vacancies existed in the surface lower its adsorption energy. Therefore, more super oxygen anion radical forms on surface of NV-TiO_2. Then, phenol transforms into other intermediate products quickly and it is not detected on surface of NV-TiO_2 sample. After reversing the calcination order,

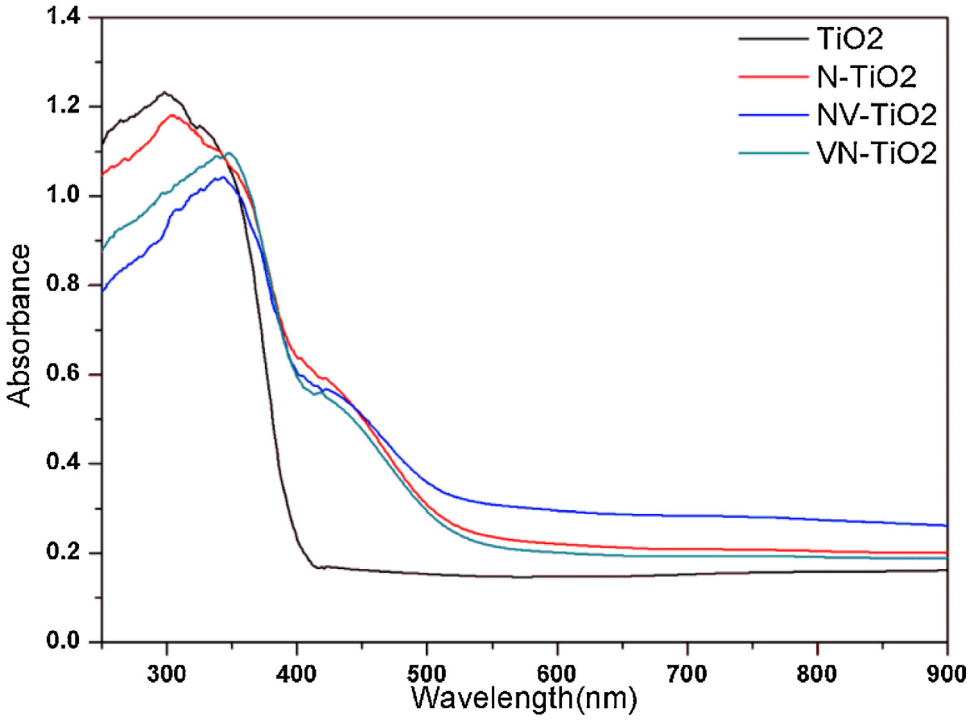

Fig. 6. UV–vis diffuse reflection spectrum for pure TiO_2, N-TiO_2, NV-TiO_2 and VN-TiO_2.

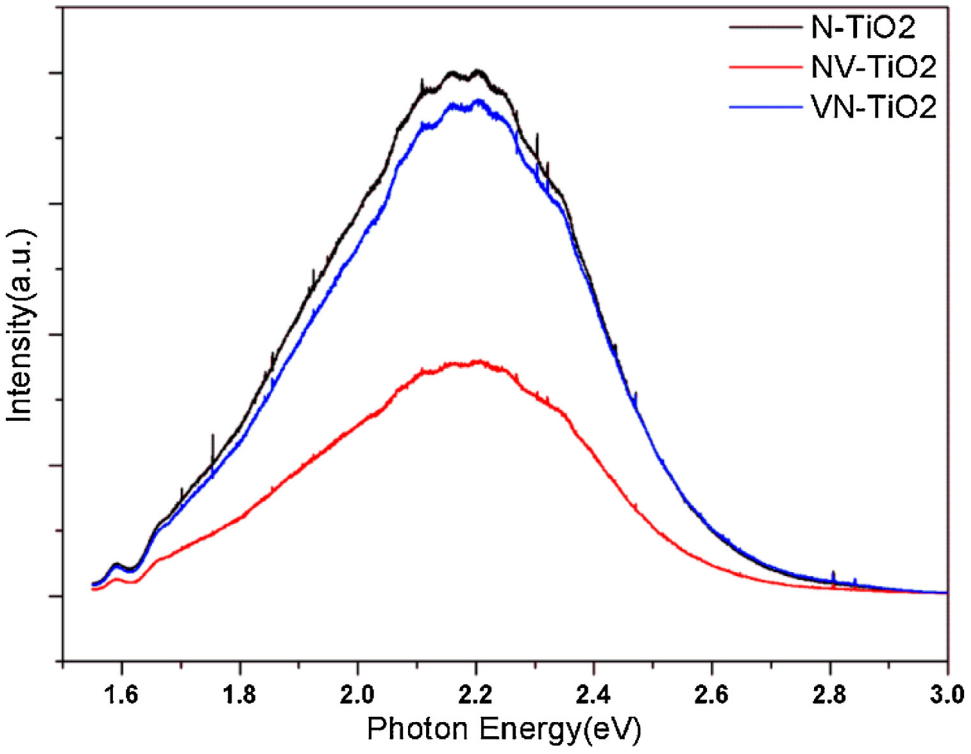

Fig. 7. PL spectra of N-TiO_2, NV-TiO_2 and VN-TiO_2. The samples were excited at 325 nm at room temperature.

the decline in amount of oxygen vacancies causes the reduction of active species. Meanwhile, the formation of surface NO_x species also causes the reduction of super oxygen anion radical in VN-TiO_2. Thus, phenol is detected in VN-TiO_2 after 10 min reaction. Similarly, the fewest oxygen vacancies generate in N-TiO_2 sample. It suggests that the active species formed on surface of N-TiO_2 is fewest. Furthermore, the recombination of electron and hole is the most serious for N-TiO_2. Therefore, the active species generated in N-TiO_2 is fewer. It is not difficult to understand that phenol still be detected after a long time reaction. In this way, the presence of phenol becomes a measurement of photocatalytic activity towards decomposing benzene. The later phenol is detected, the worse the photocatalytic activity is. In addition, the stability of photocatalyst is also tested and the result is exhibited in Fig. S5. The photocat-

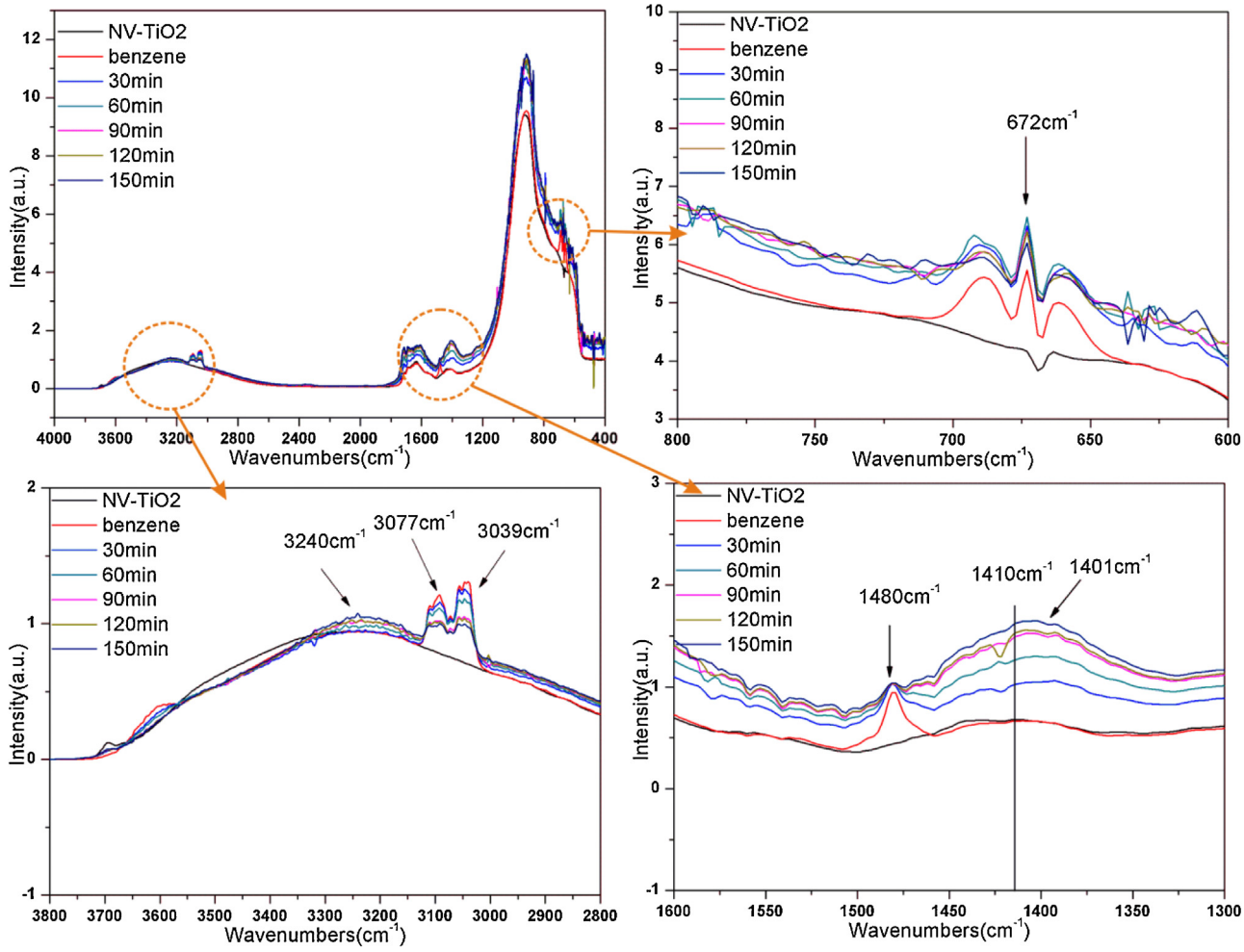

Fig. 8. In situ Fourier transform infrared spectrum of decomposing benzene over NV-TiO_2 under visible light irradiation.

alytic activity is not deteriorated obviously and the degradation efficience of benzene still remains to 95% after five repeated cycles.

4. Conclusion

In this paper, a modular calcination method to prepare modified N-doped TiO_2 nanoparticle with high photocatalytic activity was proposed. The samples prepared by annealing in ammonia and vacuum possess the best photocatalytic activity under visible light illumination. As an example, the effect of calcination order on photocatatlytic activity was explained by this combination. In addition, the excellent photocatalytic performance of NV-TiO_2 was attributed to good crystallinity, strong light harvesting and fast separation of photogenerated carriers. The improvement of charge separation was ascribed to the formation of paramagnetic $\left[O - Ti^{4+} - N^{2-} - Ti^{4+} - V_O\right]$ cluster which was detected by EPR. The surface oxygen vacancy induced by vacuum treatment trapped electron and promoted to generate super oxygen anion radical which was a necessary active species in photocatalytic process. It also has positive effect on the performance of NV-TiO_2. More importantly, the investigation of reaction path for decomposing benzene revealed that phenol was an important intermediate product and the transformation of phenol is a fast step in degradation reaction of benzene. The later phenol presented, the worse the photocatalytic activity was. In addition, the photocatalytic property of modified nitrogen doped TiO_2 prepared by other combinations exhibited the same trend as the combination of ammonia and vacuum, shown in ESI. The photocatalytic activity of modified nitrogen doped TiO_2 was better than that of N-TiO_2. And the photocatalytic activity of sample annealed in ammonia firstly is higher than the sample annealed in ammonia last. The above findings deepen us understand the mechanism of photocatalytic degradation of benzene. Besides, the proposed modular calcination method paves a new way to prepare highly efficient photocatalyst and it is also feasible for industrial production.

Conflict of interest

The authors declare no competing financial interest.

Acknowledgments

This work was financially supported by Graduate Student's Entrepreneurial Innovation Fund of Huazhong University of Science and Technology (No. 2015650011) and the National Basic Research Program of China (Grant No. 2009CB939705). The authors are also grateful to Analytic and Testing Center of Huazhong University of Science and Technology.

Appendix A. Supplementary data

Supplementary data associated with this article can be found, in the online version, at http://dx.doi.org/10.1016/j.apcatb.2015.10.048.

References

[1] A. Fujishima, K. Honda, Nature 238 (1972) 37–38.
[2] H. Einaga, T. Ibusuki, S. Futamura, J. Sol. Energy Eng. 126 (2004) 789.
[3] Y. Liu, W. Shu, K. Chen, Z. Peng, W. Chen, ACS Catal. 2 (2012) 2557–2565.
[4] Z. Liu, P. Fang, S. Wang, Y. Gao, F. Chen, F. Zheng, Y. Liu, Y. Dai, J. Mol. Catal. A Chem. 363–364 (2012) 159–165.
[5] C. Ren, X. Liu, G. Wang, S. Miao, Y. Chen, J. Mol. Catal. A Chem. 358 (2012) 31–37.
[6] Y. Hu, D. Li, Y. Zheng, W. Chen, Y. He, Y. Shao, X. Fu, G. Xiao, Appl. Catal. B Environ. 104 (2011) 30–36.
[7] D. Nassoko, Y.F. Li, H. Wang, Y.Z. Li, Y. Yu, J. Alloys Comp. 540 (2012) 228–235.
[8] H.J. Huang, D.Z. Li, Q. Lin, W.J. Zhang, Y. Shao, Y.B. Chen, M. Sun, X.Z. Fu, Environ. Sci. Technol. 43 (2009) 4164–4168.
[9] Z.Z. Zhang, X.X. Wang, J.L. Long, Q. Gu, Z.X. Ding, X.Z. Fu, J. Catal. 276 (2010) 201–214.
[10] S. Hoang, S.P. Berglund, N.T. Hahn, A.J. Bard, C.B. Mullins, J. Am. Chem. Soc. 134 (2012) 3659–3662.
[11] X.F. Chen, X.C. Wang, Y.D. Hou, J.H. Huang, L. Wu, X.Z. Fu, J. Catal. 255 (2008) 59–67.
[12] L. Zeng, L. Zhao, J. Yang, M.H. Li, W.L. Song, D.W. Zeng, C.S. Xie, Appl. Catal. B Environ. 166–167 (2015) 1–8.
[13] S. Bakardjieva, V. Stengl, L. Szatmary, J. Subrt, J. Lukac, N. Murafa, D. Niznansky, K. Cizek, J. Jirkovsky, N. Petrova, J. Mater. Chem. 16 (2006) 1709.
[14] M. Sathish, B. Viswanathan, R.P. Viswanath, C.S. Gopinath, Chem. Mater. 17 (2005) 6349–6353.
[15] S. Sakthivel, H. Kisch, Chemphyschem 4 (2003) 487–490.
[16] X.B. Chen, Y.B. Lou, A.C.S. Samia, C. Burda, J.L. Gole, Adv. Funct. Mater. 15 (2005) 41–49.
[17] R. Asahi, T. Morikawa, T. Ohwaki, K. Aoki, Y. Taga, Science 293 (2001) 269–271.
[18] A. Fujishima, X.T. Zhang, D. Tryk, Surf. Sci. Rep. 63 (2008) 515–582.
[19] J. Ananpattarachai, P. Kajitvichyanukul, S. Seraphin, J. Hazard Mater. 168 (2009) 253–261.
[20] S. Livraghi, A. Votta, M.C. Paganini, E. Giamello, Chem. Commun. 4 (2005) 498–500.
[21] C.D. Valentin, E. Finazzi, G. Pacchioni, A. Selloni, S. Livraghi, M.C. Paganini, E. Giamello, Chem. Phys. 339 (2007) 44–56.
[22] C. Di Valentin, G. Pacchioni, A. Selloni, Phys. Rev. B 70 (2004) 085116.
[23] G. Barolo, S. Livraghi, M. Chiesa, M.C. Paganini, E. Giamello, J. Phys. Chem. C 116 (2012) 20887–20894.
[24] S.V. Awate, R.K. Sahu, M.D. Kadgaonkar, R. Kumar, N.M. Gupta, Catal. Today 141 (2009) 144–151.
[25] N. Sivasankar, S. Vasudevan, J. Phys. Chem. B 108 (2004) 11585–11590.
[26] W.C. Wu, L.F. Liao, C.F. Lien, J.L. Lin, Phys. Chem. Chem. Phys. 3 (2001) 4456–4461.
[27] Y. Shen, Q.D. Zhao, X.Y. Li, D.L. Yuan, Y. Hou, S.M. Liu, J. Hazard. Mater. 241-242 (2012) 472–477.
[28] J. Arana, E.P. Melian, V.M. Rodriguez Lopez, A.P. Alonso, J.M. Dona Rodriguez, O.G. Diaz, J.P. Pena, J. Hazard. Mater. 146 (2007) 520–528.
[29] T.D. Bui, A. Kimura, S. Higashida, S. Ikeda, M. Matsumura, Appl. Catal. B Environ. 107 (2011) 119–127.
[30] J. Chen, L. Eberlein, C.H. Langford, J. Photochem. Photobiol. A Chem. 148 (2002) 183–189.
[31] H. Yuzawa, M. Aoki, K. Otake, T. Hattori, H. Itoh, H. Yoshida, J. Phys. Chem. C 116 (2012) 25376–25387.
[32] J.B. Zhong, J.L. Wang, L. Tao, M.C. Gong, Z.M. Liu, Y.Q. Chen, J. Hazard. Mater. 140 (2007) 200–204.